Laser synthesis and comparative testing of a three-dimensional porous matrix of titanium and titanium nickelide as a repository for stem cells

ARTICLE *in* POWDER METALLURGY AND METAL CERAMICS · FEBRUARY 2012

Impact Factor: 0.22 · DOI: 10.1007/s11106-012-9366-9

4 AUTHORS, INCLUDING:

Igor V. Shishkovsky
Russian Academy of Sciences
89 PUBLICATIONS **502** CITATIONS
SEE PROFILE

Iurii Georgievich Morozov
Institute of Structural Macrokinetics and M…
125 PUBLICATIONS **630** CITATIONS
SEE PROFILE

Powder Metallurgy and Metal Ceramics, Vol. 50, Nos. 9-10, January, 2012 (Russian Original Vol. 50, Nos. 9-10, Sept.-Oct., 2011)

LASER SYNTHESIS AND COMPARATIVE TESTING OF A THREE-DIMENSIONAL POROUS MATRIX OF TITANIUM AND TITANIUM NICKELIDE AS A REPOSITORY FOR STEM CELLS

I. V. Shishkovskii,[1,4] Yu. G. Morozov,[2] S. V. Fokeev,[3] and L. T. Volova[1]

UDC 621.373.826:621.762.53

The paper discusses the prospects of layer-by-layer synthesis of porous tissue scaffolds (matrices) of titanium and NiTi (nitinol) as a repository for stem cells. The experiments are performed on primary cultures of human dermal fibroblasts of 4–18 passages. The culture of dermal fibroblasts is obtained from the skin and muscle tissue of 6 to 10-week abortuses with the method of primary explants. The role of surface morphology of porous matrices of these materials in cell adhesion and proliferation is examined in comparison with cast dental titanium. The surface microstructure and roughness are analyzed with optical and scanning electron microscopy before and after experiments in vitro. The elemental analysis is used to determine the biochemical composition of post-experimental porous matrix structures. The results show high chemotaxis of cells to the samples and effect of the matrix composition on the development of cell culture.

Keywords*: titanium, nitinol, tissue scaffold, selective laser sintering, osseointegration, multipotent mesenchymal stromal cells, differentiation, bone formation, porous matrix.*

INTRODUCTION

Tissue engineering is an area of regenerative medicine that is being widely promoted and includes the cultivation of cells *in vitro*, cell biology research, development and restoration of damaged or lost tissues, control and testing, as well as the synthesis of new pharmaceutical products [1, 2]. Under this concept, it is of most interest to create (stimulate the synthesis of) tissues or organs *in vitro* by cell implantation in the extracellular matrix (ECM).

As opposite to the normal growth of cells *in vitro*, tissue scaffolds can be given a strictly individual shape for each patient that not only serves as a support but also determines the direction in which cells develop in the extracellular matrix, contributing to their differentiation and the formation of an artificial tissue. This revolutionary engineering approach to the synthesis of tissues *in vitro* corresponds to their natural development *in situ* [3–7].

In reparative surgery, it is currently important to replace cast porous implant materials by porous scaffolds (matrices) having the shape of the body (bone) to be replaced to restore the defective areas. The topography of the

[1]Lebedev Physical Institute, Russian Academy of Sciences, Samara Branch, Samara, Russia. [2]Institute of Structural Macrokinetics and Materials Science, Russian Academy of Sciences, Chernogolovka, Russia. [3]Central Research Laboratory, Samara State Medical University, Samara, Russia.

[4]To whom correspondence should be addressed; e-mail: shiv@fian.smr.ru.

Translated from Poroshkovaya Metallurgiya, Vol. 50, No. 9–10 (481), pp. 42–57, 2011. Original article submitted December 15, 2009.

 1068-1302/12/0910-0606

porous surface, as against the smooth surface, influences the morphological features of cell behavior, and cell proliferation is determined by the synergy of micro- and nanotopography [8, 9]. There is also a challenge because the cellular matrix must show biopsy characteristics throughout the pore structure in which the cellular mass will grow and new tissues will synthesize *in vitro*. Different substances may be used as the matrix material. Biologically inert materials that are nontoxic and resistant to biochemical effects of the living body (titanium, ceramics, etc.) were originally preferred.

The use of titanium in medicine is addressed in a vast number of publications that show that it is bioinert; increase in the titanium content by several orders of magnitude exerts no allergic, carcinogenic, or toxic effects [10–17]. In particular, no cytotoxic effect is observed in the interaction of porous titanium with the culture of bone marrow cells. Of great interest are bioactive porous degradable materials that include hydroxyapatite (HAP) [18–25]. These materials retain sufficient mechanical strength in the process of their replacement by bone tissue. However, in the reality, the restoration of natural bone structure is often behind the degradation of this artificial matrix.

Nitinol (intermetallic phase—NiTi) is another promising material for implantation because it has a unique combination of properties (inherent even in the porous state), including the shape memory effect (SME), high strength and corrosion resistance [9, 24, 26–39]. Moreover, the open porosity facilitates the growth of the connective tissue into the implant, thus improving the implant–bone connection. Although the alloys based on TiNi are not subject to significant corrosion (because passivation in biological fluids leads to a layer containing a small amount of nickel), the problem of their biocompatibility cannot be regarded as solved [37], since this intermetallic compound includes about 50 at.% Ni. Nickel is known to be a toxic element that has allergenic and carcinogenic effects, and about 15% of people have an increased sensitivity to it. This metal as Ni^{2+} ions has a strong chemotactic effect on the body's cells and is a biocatalyst accelerating the destruction of blood plasma proteins. Implantation of nickel into the body shows carcinogenic activity of Ni^{2+} ions and a broad zone of inflammatory processes associated with the dissolution of nickel in tissue fluids.

The Rapid Prototyping and Manufacturing technology has an undeniable medical potential since individual implants can be created with a predetermined internal and (or) external surface shape. The advantage of selective laser sintering (SLS) relating to this technology is the creation of functional implants using three-dimensional computer tomography without any extra molding operations [1, 2, 10–11, 15–17, 23, 25, 40–51]. The control and design of the internal structure of pore channels at the stage of computer modeling allow intensive growth of connective tissues into the porous matrix and increase in the contact area (and, hence, the mechanical strength) between the implant and bone. Porous channels can be saturated with drugs to activate the process of implantation, preventing cell death [1, 6].

The objective is to study the properties of a porous implant material consisting of titanium, nitinol, and additions of hydroxyapatite to these materials as a three-dimensional matrix for stem cells, as compared with cast titanium conventionally used in dentistry. Results are presented for cell adhesion, proliferation, and differentiation for three-dimensional tissue matrices (scaffolds) of these materials, along with results from studies of cellular morphology by optical and scanning electron microscopy.

EXPERIMENTAL PROCEDURE

The nitinol powders (NiTi phase >99.7 wt.%) of P55H45 grade and titanium powders (Ti > 98.1 wt.%) of PTOM grade were purchased at the *Polema* Company (Tula, Russia). Prior to laser sintering, the powders were dried in a vacuum oven for 2 h at 300°C. In a series of experiments, we added hydroxyapatite of grade GAP-85d (*Intermedapatit* Company, Moscow) to the powders to increase their biocompatibility. For reference, we used cast titanium of the *Rema* Company, which is widely used in dentistry. The particle size of all starting powders was ~100 μm (to be commensurate with the diameter of the laser spot) and was checked with a sieve analysis. As a result of laser sintering, three-dimensional flat porous matrix samples about 10 mm × 10 mm in size with a monolayer about 0.5–1 mm thick depending on the mode of laser sintering were formed for biological tests. Figure 1*a* shows the appearance of a porous titanium matrix and Fig. 1*b* a porous nitinol tissue scaffold of cell type, whose structure was designed on the computer.

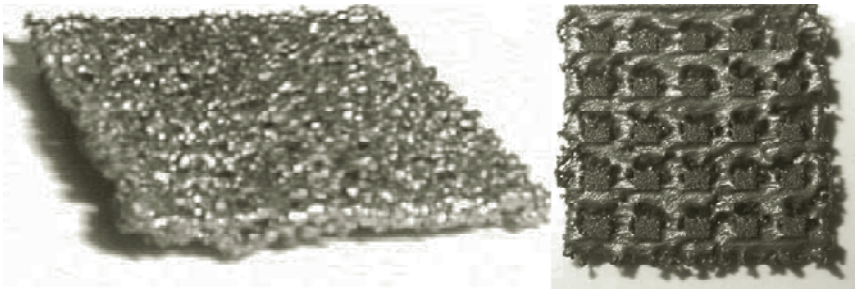

a *b*

Fig. 1. Tissue scaffolds 10 mm ×10 mm in size: *a*) titanium, side view, chaotic porosity; *b*) nitinol, top view, regular porosity

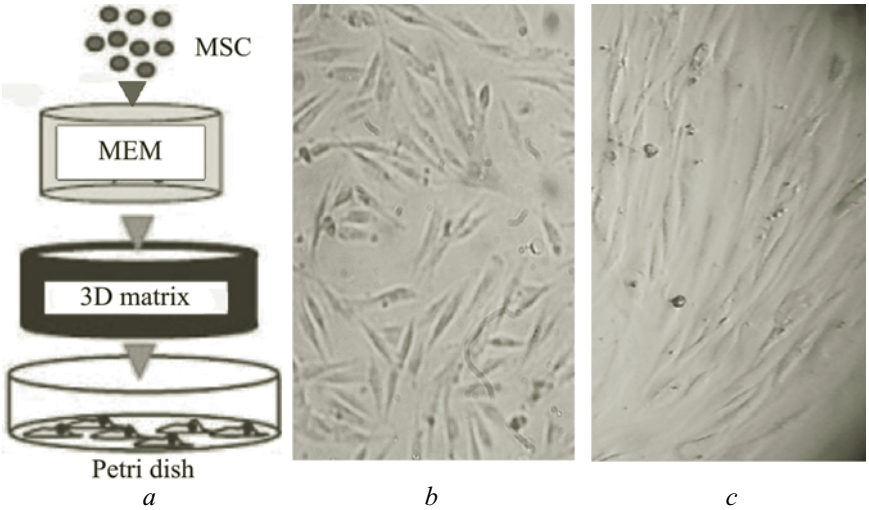

a *b* *c*

Fig. 2. Experimental setup (*a*) and primary cell culture of human embryos: *b*) mesenchymal stromal cells from skull roof; *c*) dermal fibroblasts, native products; ×150

The morphological study was conducted at the Central Research Laboratory, Samara State Medical University (Russia), on primary cultures of human dermal fibroblasts of the 4^{th}–18^{th} passages. The culture of dermal fibroblasts was obtained from skin and muscle tissues of 6 to 10-week abortuses using primary explants. Multipotent mesenchymal stromal cells (MMSC) were cultured in standard conditions: Sanyo-Incubator MIR-262 thermostat, 37°C, 100% humidity, 5% CO_2, α-MEM medium (Minimum Essential Medium Eagle) with 10% fetal calf serum, Orange Scientific (Belgium) and Corning (USA) plastic culture flasks, and 25 cm^2 area. The experiments were carried out in Petri dishes (Sarstedt) with a diameter of 3 cm.

The experiments were carried out using the direct contact method and two options (Fig. 2*a*): 1) fibroblasts were passaged from culture flasks to Petri dishes and cultured for 24 h (during this time, a cell monolayer formed with a density of ~315 cells/mm^2, onto which the test sample was placed) and 2) fibroblasts were passaged into culture dishes and the test sample was placed there immediately. The dose of cells (in all cases) remained unchanged (2×10^4 cells/cm^2). This was verified in both cases as follows: Petri dishes with complete growth medium and samples of test material without any fibroblasts; Petri dishes with the culture of fibroblasts which were passaged and placed simultaneously with the test samples but not subjected to any action. To collect statistics, five samples were used for each option. Cells in the presence of the test material were cultured for four to six days.

The native culture was studied, subjected to morphometry, and photographed using a Biolam P-2-1 inverted microscope at 100- and 150-fold magnification. The material was stained with hematoxylin eosin. The native culture was visually observed and subjected to morphometry every day. We visually assessed the integrity of the monolayer, the presence of desquamated (dead) cells in the culture medium, and the shape and size of cells and

evaluated the cytotoxic effect and the efficiency of attachment and proliferation. The culture medium was passaged into the test and reference flasks to determine the content of total protein, protein-free, and protein-bound oxyproline with the microbiuretic method [52]. Statistical treatment was performed using parametric and nonparametric criteria for reliability analysis.

We analyzed the structure of pore space and chemical composition of the sintered samples before and after experiments *in vitro*. Optical and scanning electron microscopy (SEM) (LEO 1450, Carl Zeiss, with an EDX-Energy Dispersive X-ray Microanalyzer, INCA Energy 300, Oxford Instruments) was used. To study the cell layer on the matrix surface with SEM, the samples with cells were fixed in a 2.5% solution of glutaric aldehyde, dehydrated, and dried at a Hitachi HCP-2 Critical Point Drier.

EXPERIMENTAL RESULTS AND DISCUSSION

Sterilization of the material. Fibroblasts in a normal primary culture are usually elongated and have two to four processes and homogeneous cytoplasm, the cell borders are distinct, the nucleus is located eccentrically and contains one to three nucleoli (Fig. 2*b*, *c*). The cells which were on cover glass at the center of Petri dishes uniformly proliferated and migrated to the bottom of the dish along the entire perimeter for the period of observation. The dominant elements are rounded cells that are transformed into different cell lines.

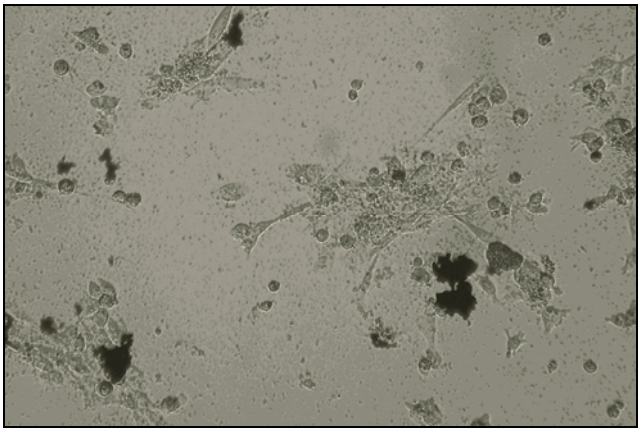

Fig. 3. Broken edges of the titanium nickelide (NiTi) sample on a monolayer of fibroblasts; bacterial contamination of the dish after single sterilization of the test material; desquamated cells; four days of the experiment; cell death; ×150

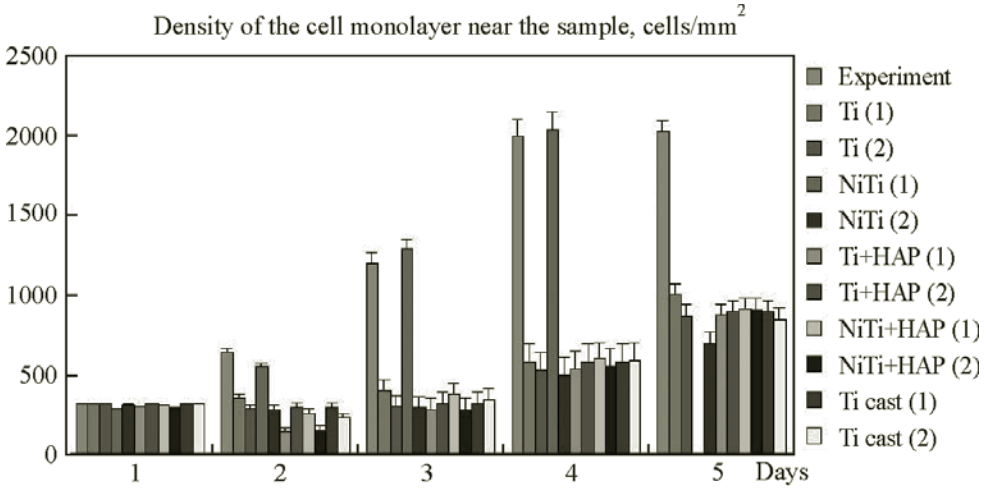

Fig. 4. The density of the monolayer near the sample by days of experiment: here and below in Figs. 5 and 6, the brackets by the sample material show the number of experiment option; the vertical lines indicate the estimated standard deviation from the mean

The first step was to develop methods for sterilization of the material obtained. Since the porous matrix was not initially sterile, it was processed according to rules for treatment of surgical instruments; that is, it was soaked for one day in a chloramine solution and then thoroughly washed, dried, and sterilized in a dry heat oven at 200°C for 3 h. Despite this, in all the dishes containing samples of the material treated only once (as in the experimental culture of fibroblasts and reference), the growth medium became clouded in 24 h, its pH changed to the acid side (to 4.5–4.8), and cells desquamated into the medium (Fig. 3). This is evidence of significant bacterial contamination of the samples, which could not be eliminated through conventional treatment and sterilization.

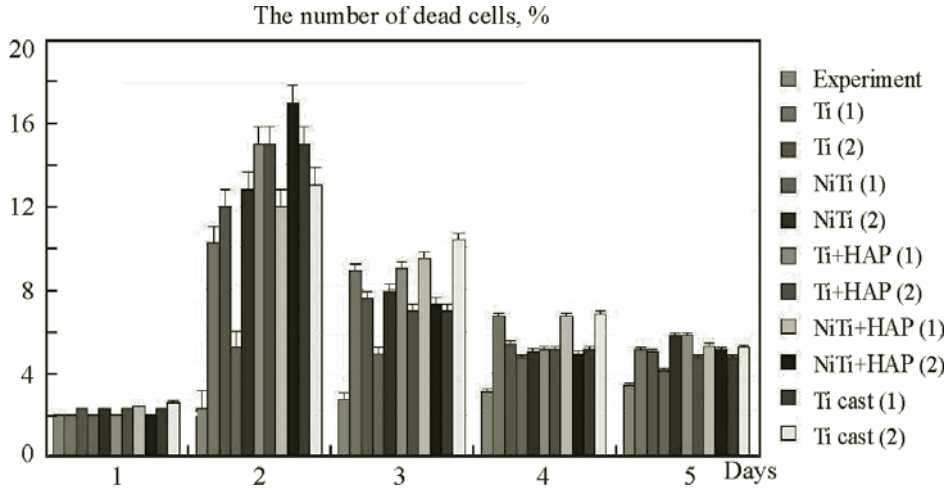

Fig. 5. The number of damaged cells by days of experiment for the test materials and experiment options

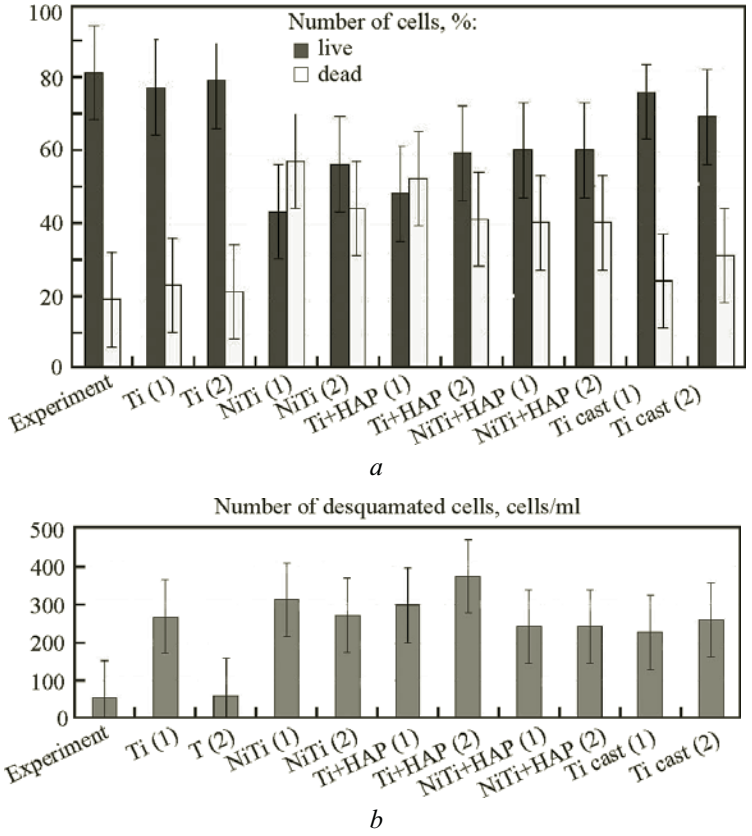

Fig. 6. The ratio of live and dead cells (*a*) and the number of desquamated cells (*b*) by the end of experiment

In this regard, we had to subject the samples to a threefold cycle of sterilization. In this case, the samples that were in the thermostat in complete growth medium did not cause the growth of bacterial flora.

Quantitative assessment of cell adhesion and proliferation. Statistical treatment of morphological data for stem cells in SLS porous scaffolds proceeds as follows. Figure 4 shows the adhesion of osteoblasts near the surface of the porous matrix by days of experiments. The reference line characterizes the behavior of fibroblasts in the growth medium without any external influence. The medium is almost as dense as the fibroblasts on the surface of nitinol for the first option of experiment. In general, all samples stimulate the proliferation of fibroblasts. As compared with the initial density of ~315 cells/mm^2, the cell population is always doubled and tripled, which indicates the effectiveness of their adhesion to the surface of the samples.

The number of dead cells (Fig. 5) is also minimum for NiTi (option 1). A good result is shown by the porous titanium matrix (option 1). Moreover, the number of dead cells is quite significant, but less than in other cases. We attribute the massive cell death on the second day of the experiment (the characteristic peak in Fig. 5) to stress response to the introduction of samples and cell damage due to this external influence. On the subsequent days, regeneration started, and the number of dead cells decreased. It is important to note that the addition of HAP did not significantly affect the behavior of fibroblasts at the surface of the porous matrix.

Figure 6*a* shows the percentage of live and dead cells by the end of the experiment. The number of dead cells (57%) insignificantly exceeds the number of live cells (43%) only for the nitinol matrix (option 1) and Ti + HAP porous scaffold (option 1). Meanwhile, the growth dynamics of stem cells for this case was the most favorable. In other cases, the number of live cells is greater than the number of dead ones. The best results, comparable to reference, were observed for the titanium matrix. The number of desquamated cells by the end of the experiment is characterized in Fig. 6*b*. The total number of desquamated cells is minimum for reference and porous titanium matrix (option 2); their most critical number is shown by NiTi (option 1) and Ti + HAP (option 2).

Optical microscopy of cell distribution. Typical microphotographs of the contact surface of SLS porous matrices, mainly in the late (5–6 days) stages of the experiment, are shown in Fig. 7*b–f*. For comparison, Fig. 7*a* shows a sample of porous titanium on the first day of experiments. Noteworthy is the decrease in the density of a

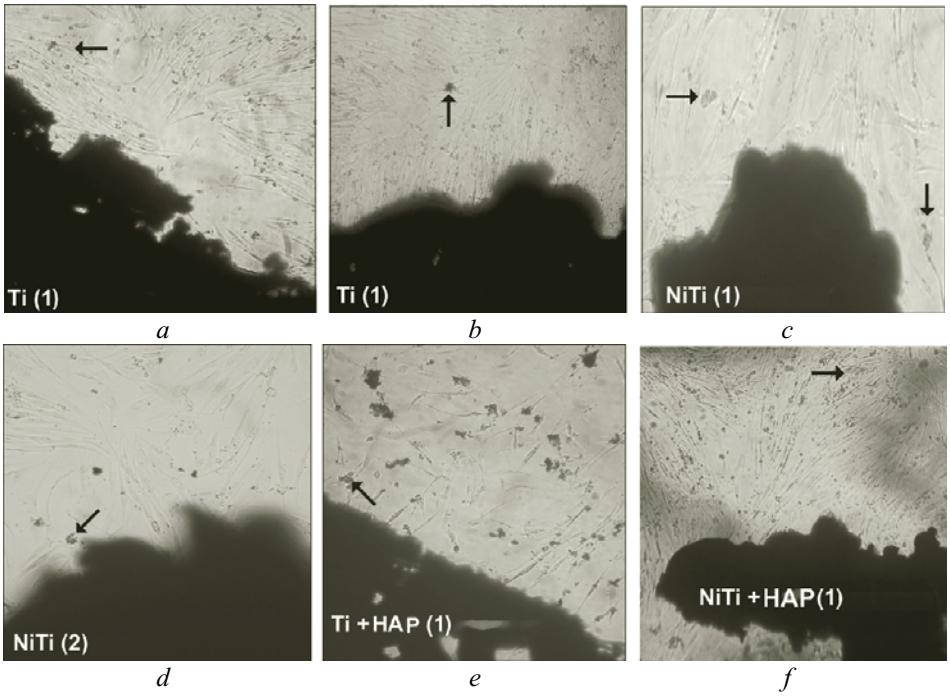

a *b* *c*

d *e* *f*

Fig. 7. Edge of the samples of porous scaffolds on a monolayer of fibroblasts: at the corner, the photograph (black) shows the test samples; native culture; the arrows indicate to desquamated cells; inverted microscope; ×100

fibroblast monolayer in the immediate vicinity of the sample due to its damage by broken pieces of titanium. The stem cells are elongated, densely packed, and tend to lie in parallel to the surface. However, on the fifth or sixth day (Fig. 7*b*), there is adhesion of MMSC to the test material. The cells are arranged and grow perpendicularly into the pores of the sample. The same is observed for nitinol (Fig. 7*c*) on the fifth day. The cell density near the sample is not so great; some number of desquamated cells (indicated by arrows) should be noted. Figure 7*d* shows the native structure of fibroblasts at the surface of nitinol (option 2) on the sixth day of experiments. Lines of fibroblasts are both perpendicular and oblique to the matrix surface. Addition of HAP increases the fragility of the matrix edges (see the discussion of Fig. 8*d*). Figure 7*e* shows pieces broken off from the sample. However, the proliferative activity of MMSC, especially in the case of NiTi + HAP, is very high, as can be judged from the orientation of proliferated cells.

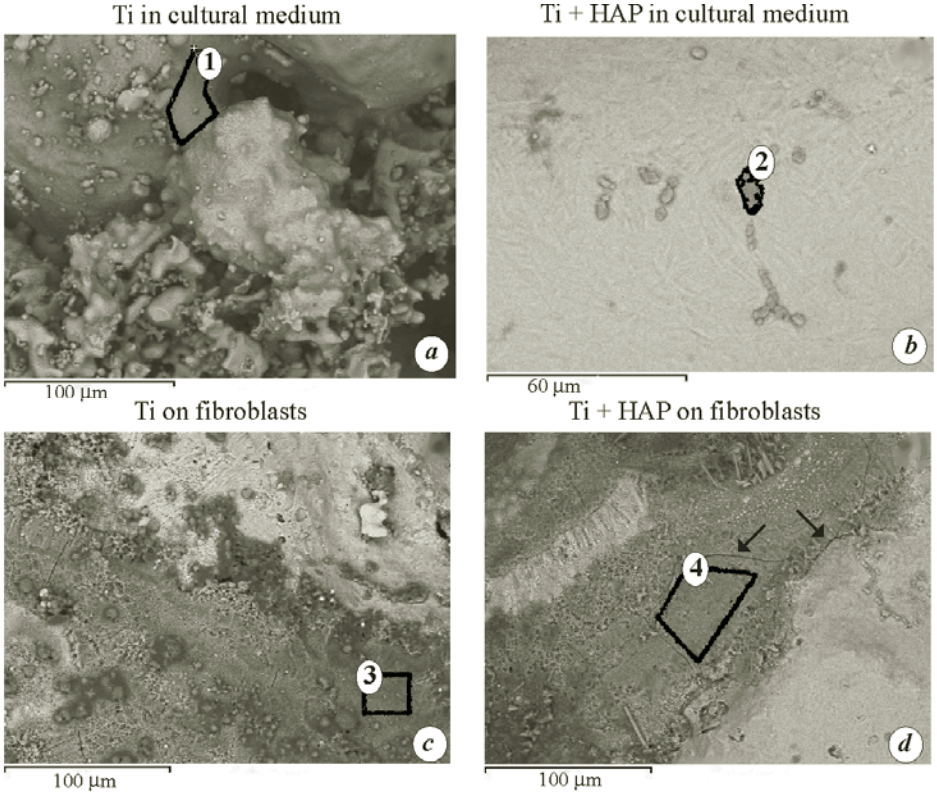

Fig. 8. Scanning electron microscopy of fibroblasts on porous titanium microstructures: here and below in Figs. 9 and 10, a loop with a figure denote the area used for EDX microanalysis

TABLE 1. EDX Microanalysis on the Areas of Titanium Implant Indicated in Fig. 8

Element	Content of elements, at.%, at point			
	1 (Fig. 8*a*)	2 (Fig. 8*b*)	3 (Fig. 8*c*)	4 (Fig. 8*d*)
C	8.61	8.26	11.89	13.78
O	64.04	25.94	60.45	58.76
Na	–	21.16	–	1.65
Al	0.91	1.48	0.74	1.00
P	–	0.56	0.76	0.72
Cl	–	11.56	0.29	0.82
Ca	0.58	0.49	11.59	9.68
Ti	25.86	30.56	14.28	13.59

It has been established in the cultivation process that fibroblast-like elements are predominant on the fifth or sixth day, and then elements of the differentiating factor that was added prevail. After that, individual centers, characterized by attachment to titanium or nitinol pore walls, merge and form a cell monolayer in pores. For culturing *in vivo*, we previously noted stable growth of chondrogenic and osteogenic elements in the pores of titanium and titanium nickelide [40]. Colonies of osteoblasts in the pores of TiNi form a chondrogenic or bone matrix.

For the cast sample, we observed cell growth mainly near grinding defects. Fibroblasts were concentrated in the direction of titanium. By the end of the experiment, we noticed the degeneration of cells. Their morphology also corresponded to the growth period: the cells were spindle-shaped with a homogeneous cytoplasm and centrally located bubble-like nucleus and did not closely fit to each other and had anastomotic processes.

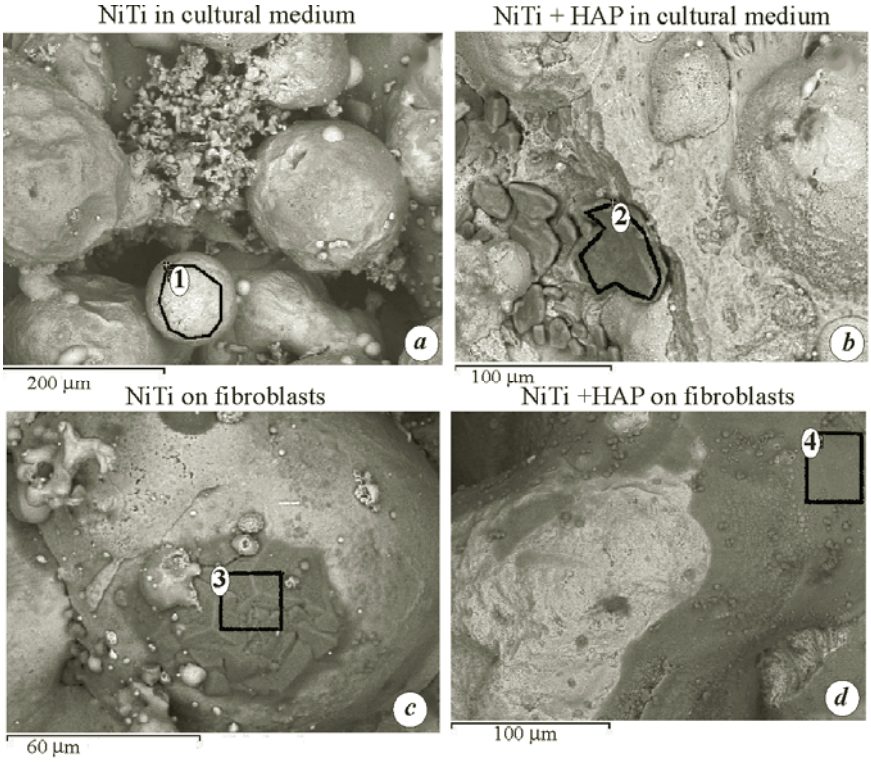

Fig. 9. Scanning electron microscopy of fibroblasts on porous nitinol microstructures

TABLE 2. EDX Microanalysis on the Areas of Nitinol Implant Indicated in Fig. 9

Element	Content of elements, at.%, at point			
	1 (Fig. 9*a*)	2 (Fig. 9*b*)	3 (Fig. 9*c*)	4 (Fig. 9*d*)
C	14.75	–	9.12	12.84
O	43.35	7.78	55.91	51.03
Mg	–	–	0.80	–
Al	–	–	0.72	–
Na	–	48.31	–	1.78
P	–	0.78	4.52	0.81
Cl	–	41.01	0.35	0.73
Ca	0.56	–	14.25	15.37
Ti	26.41	1.45	14.33	17.44
Ni	14.93	0.67	–	–

Scanning electron microscopy. Analysis of the surface topography of the sintered titanium powder shows (Fig. 8*a*) that its structure belongs to a typical spongy morphological type, the smooth surfaces of the particles have rounded protuberances about 10 to 30 μm in size. After SLS, the powder particles form a matrix with open pores ranging from 50 to 200 μm. The pores are of uncertain shape and have morphologically developed surfaces, largely following the surface shape and type of initial particles. The porosity of the sintered material was 50–65%, depending on the sintering conditions [40]. In Figs. 8 and 9, the areas containing cellular structures are darker since they were photographed in backscattered radiation. The fibroblasts almost continuously cover the porous matrix surface (Fig. 8*a*, *c*) in case of pure titanium but, after addition of HAP, they are fragmentary, located probably where HAP is concentrated (Fig. 8*b*, *d*). Furthermore, the addition of HAP makes the surface more fragile (arrows in Fig. 8*d* indicate to cracks).

Data of EDX analysis are presented in Table 1, and Fig. 8 shows the area of EDX analysis with a figure. The analysis shows that the concentration of main impurity elements corresponds to their content of the starting powder. The presence of aluminum on the majority of areas is attributed to the effect of aluminum foil on the results that was used to fix the samples in the camera. The white surface coating seen on the SEM image obviously indicates the formation of titanium oxide. Thus, sintered titanium fully follows the composition of the starting powder. The presence of carbon probably indicates the presence of organics (growth medium for fibroblasts). Noteworthy is the presence of cells in the culture that produce alkaline phosphatase, which is a marker of stem cells and osteogenic cells [1]. The accumulation of calcium is most clearly seen in Fig. 8*c*, *d*. An important parameter of biocompatibility is the Ca/P ratio, which should be attributed to the addition of HAP in SLS of the titanium matrix. The presence of sodium indicates the activity of fibroblasts in pure titanium.

The microstructure of the laser-sintered nitinol (Fig. 9*a*) is also spongy, with a developed system of pores. A large amount of oxygen indicates the release of titanium from TiNi and its subsequent active oxidation to Ti_2O.

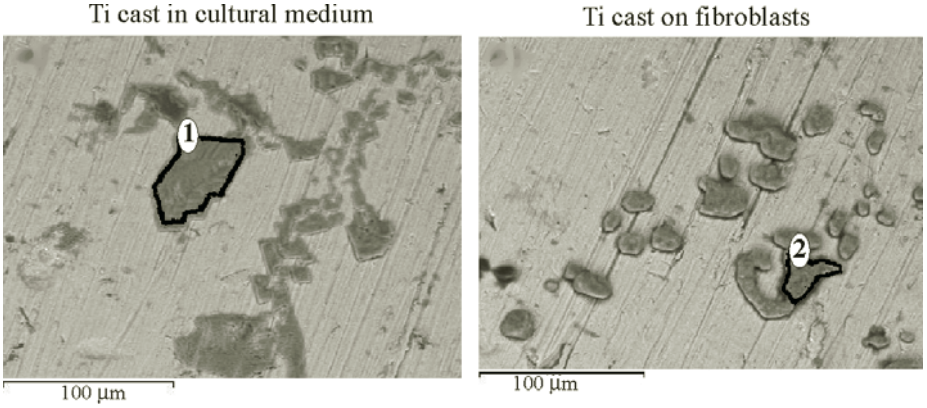

Fig. 10. Scanning electron microscopy of fibroblasts on cast titanium microstructures

TABLE 3. EDX Microanalysis on the Areas of Cast Titanium Implant Indicated in Fig. 10

Element	Content of elements, at.%, at point	
	1 (Fig. 10*a*)	2 (Fig. 10*b*)
C	15.42	43.49
O	9.37	5.77
Na	32.01	21.18
K	–	0.32
Cl	23.75	28.26
Ti	19.45	0.98

The general white coating in Fig. 9 confirms this fact. The titanium/nickel ratio (the last two rows in Table 2) corresponds to the starting powder of the intermetallic phase (nitinol). In areas of microanalysis in Fig. 9*b–d*, nickel is virtually absent on the surface. The particle size is also commensurable with the size of the starting fraction. In the medium of stem cells (Fig. 9*c*), organic matter (darker color) is clearly seen at interfaces. The ratio of elements—chlorine, phosphorus, and sodium (Table 2, Fig. 9*b*)—suggests the presence of sodium salts and alkaline phosphatase. Hydroxyapatite increases the adhesion of organic materials to nitinol. Fibroblasts almost completely (Fig. 9*d*) cover the surface of nitinol.

The arrangement of fibroblasts on cast titanium is shown in Fig. 10. It is seen that the smooth polished surface of titanium hardly promotes the attachment of cells; cell accumulations are seen only in places of polishing scratches. However, the production of alkaline phosphatase (Table 3) probably takes place as well. Due to the "smoothness," the cast sample "moved" along the growth medium, which made the assessment difficult.

CONCLUSIONS

The paper presents comparative results of morphological analysis of the growth of stem cells on porous matrices created by selective laser sintering on titanium and nitinol for tissue engineering. It is obvious that the creation of tissue scaffolds (for example, for oral and maxillofacial surgery) is relevant and promising.

Selective laser sintering permits layer-by-layer synthesis of titanium or nitinol implants that are not cytotoxic, which is evidenced by pronounced cell adhesion in the presence of the implant and good condition of the monolayer in the area adjacent to the sample with a high density of cells. The cells retain their structural and proliferative activity.

Porous matrices based on Ti, NiTi, Ti + HAP, and NiTi + HAP have so well developed porosity that, on the one hand, it opens up broad prospects for the effects of growth and adhesion and, on the other hand, creates issues related to the strength of these products.

The two options for stem cell proliferation are characterized by high chemotaxis of the cells to the samples, which decreases the number of cells in intermediate areas.

The presence of hydroxyapatite does not significantly influence the cell reproduction, indicating the actual high biocompatibility of titanium or nitinol. The nature of cell growth suggests that titanium is rather a biotolerant material for implantation, while nitinol is a biocompatible material.

The damaging effect of fibroblasts on the first day of experiments and the inadequate mechanical strength of porous scaffolds do not allow them to be recommended as a universal material for substrate matrices. Despite these drawbacks, these materials can compete with organotypic polymers. In future, laser sintering should be turned to layer-by-layer fusion of such implants, which will allow their use for replacement of skin, cartilage, and bone defects in surgical practices.

ACKNOWLEDGEMENTS

The research was sponsored from the Russian Fundamental Research Fund (Project No. 10-08-00208-a) and Grant under the *Fundamental Sciences to Medicine* Program of the Russian Academy of Sciences (stages for 2009–2011).

REFERENCES

1. J. M. Kanczler, S. Mirmalek-Sani, N. A. Hanley, et al., "Biocompatibility and osteogenic potential of human fetal femur-derived cells on surface selective laser sintered scaffolds," *Acta Biomater.*, **5**, 2063–2071 (2009).
2. K. F. Leong, K. K. S. Phua, C. K. Chua, et al., "Fabrication of porous polymeric matrix drug delivery devices using the selective laser sintering technique," *Proc. Inst. Mech. Eng. Part H*, **215**, 191–201 (2001).
3. E. Behravesh, A. Yasko, P. Angel, and A. Mikos, "Synthetic biodegradable polymers for orthopedic applications," *Clin. Orthop.*, **367S**, 118–185 (1999).

4. K. J. L. Burg, S. Porter, and J. F. Kellam, "Biomaterials development for bone tissue engineering," *Biomaterials*, **21**, 2347–2359 (2000).
5. H. L. Allcock, A. A. Ambroso, M. Attawia, et al., "A highly porous 3-dimensional polyphophazene polymer matrix for skeletal tissue regeneration," *J. Biomed. Mater. Res.*, **30**, 133–138 (1996).
6. N. Ogura, M. Kawada, W. Chang, et al., "Differentiation of the human mesenchymal stem cells derived from bone marrow and enhancement of cell attachment by fibronectin," *J. Oral Sci.*, **46**, No. 4, 207–213 (2004).
7. V. I. Itin, G. A. Pribytkov, I. A. Khlusov, et al., "Implant as a carrier of cell material of porous permeable titanium," *Kletochn. Transplantol. Tkan. Inzhener.*, **5**, No. 3, 59–63 (2006).
8. O. Zinger, K. Anselme, A. Denzer, et al., "Time-dependent morphology and adhesion of osteoblastic cells on titanium model surfaces featuring scale-resolved topography," *Biomaterials*, **25**, No. 14, 2695–2711 (2004).
9. I. V. Shishkovsky, Y. Morozov, and I. Smurov, "Nanostructural self-organization under selective laser sintering on exothermal powder mixtures," *Appl. Surf. Sci.*, **255**, No. 10, 5565–5568 (2009).
10. N. K. Tolochko, V. V. Savich, T. Laoui, et al., "Dental root implants produced by the combined selective laser sintering/melting of titanium powders," *Proc. Inst. Mech. Eng. Part L: J. Mater.: Des. Appl.*, **216**, 267–270 (2002).
11. T. Hayashi, K. Maekawa, M. Tamura, and K. Hanyu, "Selective laser sintering method using titanium powder sheet toward fabrication of porous bone substitutes," *Jap. SME Int. J. Ser. A*, **48**, No. 1, 369–275 (2005).
12. H. Nakamura, L. Saruwatari, H. Aita, et al., "Molecular and biomechanical characterization of mineralized tissue by dental pulp cells on titanium," *J. Dent. Res.*, **84**, No. 6, 515–520 (2005).
13. A. Joob-Fancsaly, T. Divinyi, A. Fazekas, et al., "Pulsed laser-induced micro- and nanosized morphology and composition of titanium dental implants," *Smart Mater. Struct.*, **11**, 819–824 (2002).
14. H.-M. Kim, H. Takadama, F. Miyaji, et al., "Formation of bioactive functionally graded structure on Ti-6Al-4V alloy by chemical surface treatment," *J. Mater. Sci.: Mater. Med.*, **11**, 555–559 (2000).
15. P. Fischer, V. Romano, H. P. Weber, et al., "Sintering of commercially pure titanium powder with a Nd:YAG laser source," *Acta Mater.*, **51**, 1651–1662 (2003).
16. B. Engel and D. L. Bourell, "Titanium alloy powder preparation for SLS," *Rapid Prototyping J.*, **6**, 97–106 (2000).
17. U. Suman Das, M. Wohlert, J. J. Beaman, and D. L. Bourell, "Processing of titanium net shapes by SLS/HIP," *Mater. Des.*, **20**, 115–121 (1999).
18. P. Buma, P. J. M. van Loon, H. Versleyen, et al., "Histological and biomechanical analysis of bone and interface reactions around hydroxyapatite coated intramedullarv implants of different stiffness: a pilot study on the goat," *Biomaterials*, **18**, No. 1, 251–1260 (1997).
19. Y. Cai, Y. Liu, W. Yan, et al., "Role of hydroxyapatite nanoparticle size in bone cell proliferation," *J. Mater. Chemistry*, **17**, No. 36, 3780–3787 (2007).
20. E. Tsuruga, H. Takita, H. Itoh, et al., "Pore size of porous hydroxyapatite as the cell-substratum controls BMP-induced osteogenesis," *J. Biochemistry*, **121**, No. 2, 317–324 (1997).
21. R. Rose, L. A. Cyster, D. M. Grant, et al., "In vitro assessment of cell penetration into porous hydroxyapatite scaffolds with a central aligned channel," *Biomaterials*, **25**, 5507–5514 (2004).
22. V. Salih, G. Georgiou, J. C. Knowles, and I. Olsen, "Glass reinforced hydroxyapatite for hard tissue surgery. Part II: in vitro evaluation of bone cell growth and function," *Biomaterials*, **22**, 2817–2824 (2001).
23. C. K. Chua, K. F. Leong, K. H. Tan, et al., "Development of tissue scaffolds using selective laser sintering of polyvinyl alcohol/hydroxyapatite," *J. Mat. Sci.: Mater. Med.*, **15**, 1113–1121 (2004).
24. H. C. Jiang and L. J. Rong, "Effect of hydroxyapatite coating on nickel release of the porous NiTi shape memory alloy fabricated by SHS method," *Surf. Coat. Techn.*, **201**, 1017–1021 (2006).

25. F. E. Wiria, K. F. Leong, C. K. Chua, and Y. Liu, "Poly-ε-caprolactone/hydroxyapatite for tissue engineering scaffold fabrication via selective laser sintering," *Acta Biomaterialia*, **3**, 1–12 (2007).
26. V. É. Gyunter (ed.), *Shape-Memory Medical Materials and Implants* [in Russian], Izd. Tomsk. Univ., Tomsk (1998), p. 487.
27. H. C. Man, Z. D. Cui, and T. M. Yue, "Corrosion properties of laser surface melted NiTi shape memory alloy," *Scripta Mater.*, **45**, 1447–1453 (2001).
28. M. Kohl, M. Bram, H.-P. Buchkremer, et al., "Production of highly porous near-net-shape NiTi components for biomedical application," in: *Proc. 5th Int. Conf. Porous Metals and Metallic Foams (MetFoam 2007)*, Canada, Montreal (2008), pp. 295–298.
29. A. Michiard, E. Engel, and C. Aparicio, "Oxidized NiTi surfaces enhance differentiation of osteoblast-like cells," *J. Biomed. Mater. Res. Part A*, **85**, No. 1, 108–114 (2008).
30. B. Clarke, P. Kingshott, and X. Hou, "Effect of nitinol wire surface properties on albumin adsorption," *Acta Biomaterialia*, **3**, 103–111 (2007).
31. J. Kapanen, A. Ilvesaro J. Danilov, et al., "Behavior of Nitinol in osteoblast-like ROS-17 cell cultures," *Biomaterials*, **23**, 645–650 (2002).
32. S. Kujalaa, A. Pajala, M. Kallioinen, et al., "Biocompatibility and strength properties of nitinol shape memory alloy suture in rabbit tendon," *Biomaterials*, **25**, 353–358 (2004).
33. C. Y. Li, X. J. Yang, L. Y. Zhang, et al., "In vivo histological evaluation of bioactive NiTi alloy after two years implantation," *Mater. Sci. Eng.*, **C27**, 122–126 (2007).
34. S. W. Robertson and R. O. Ritchie, "In vitro fatigue–crack growth and fracture toughness behavior of thin-walled superelastic Nitinol tube for endovascular stents: A basis for defining the effect of crack-like defects," *Biomaterials*, **28**, 700–709 (2007).
35. T. D. Sargeant, M. S. Raoa, C.-Y. Koh, and S. I. Stuppa, "Covalent functionalization of NiTi surfaces with bioactive peptide amphiphile nanofibers," *Biomaterials*, **29**, 1085–1098 (2008).
36. P. Sevilla, C. Aparicio, J. A. Planell, and F. J. Gil, "Comparison of the mechanical properties between tantalum and nickel–titanium foams implant materials for bone ingrowth applications," *J. Alloys Compd.*, **439**, 67–73 (2007).
37. S. Shabalovskaya, J. Anderegg, and J. van Humbeeck, "Critical overview of Nitinol surfaces and their modifications for medical applications," *Acta Biomaterialia*, **4**, 447–67 (2008).
38. C. Wirth, V. Comte, C. Lagneau, et al., "Nitinol surface roughness modulates in vitro cell response: a comparison between fibroblasts and osteoblasts," *Mater. Sci. Eng.*, **C25**, 51–60 (2005).
39. S. Wu, X. Liu, Y. L. Chan, et al., "In vitro bioactivity and osteoblast response on chemically modified biomedical porous NiTi synthesized by capsule-free hot isostatic pressing," *Surf. Coat. Technol.*, **202**, 2458–2462 (2008).
40. I. V. Shishkovskii, *Laser Synthesis of Functional Mesostructures and Bulk Parts* [in Russian], Fizmatlit, Moscow (2009), p. 424.
41. R. Bibb, D. Eggbeer, and R. Williams, "Rapid manufacture of removable partial denture frameworks," *Rapid Prototyping J.*, **12**, No. 2, 95–99 (2006).
42. J. He, D. Li, B. Lu, et al., "Custom fabrication of a composite hemi-knee joint based on rapid prototyping," *Rapid Prototyping J.*, **12**, No. 4, 198–205 (2006).
43. D. Ibrahim, T. L. Broilo, C. Heitz, et al., "Dimensional error of selective laser sintering, three-dimensional printing and PolyJet models in the reproduction of mandibular anatomy," *J. Cranio-Maxillofac. Surg.*, **37**, 167–173 (2009).
44. C. Leiggener, E. Messo, A. Thor, et al., "A selective laser sintering guide for transferring a virtual plan to real time surgery in composite mandibular reconstruction with free fibula osseous flaps," *Int. J. Oral Maxillofac. Surg.*, **38**, 187–192 (2009).
45. X. Li, J. Wang, L. L. Shaw, and T. B. Cameron, "Laser densification of extruded dental porcelain bodies in multi-material laser densification process," *Rapid Prototyping J.*, **11**, No. 1, 52–58 (2005).

46. C. B. Pham, K. F. Leong, T. C. Lim, and K. S. Chian, "Rapid freeze prototyping technique in bio-plotters for tissue scaffold fabrication," *Rapid Prototyping J.*, **14**, No. 4, 246–253 (2008).
47. J. T. Rimell and P. M. Marquis, "Selective laser sintering of ultra high molecular weight polyethylene for clinical applications," *Inc. J. Biomed. Mater. Res. (Appl Biomater.)*, **53**, 414–420 (2000).
48. J. M. Taboas, R. D. Maddox, P. H. Krebsbach, and S. J. Hollisterc, "Indirect solid free form fabrication of local and global porous, biomimetic and composite 3D polymer-ceramic scaffolds," *Biomaterials*, **24**, 181–194 (2003).
49. B. Vandenbroucke and J.-P. Kruth, "Selective laser melting of biocompatible metals for rapid manufacturing of medical parts," *Rapid Prototyping J.*, **13**, No. 4, 196–203 (2007).
50. J. M. Williams, A. I. Adewunmi, R. M. Schek, et al., "Bone tissue engineering using polycaprolactone scaffolds fabricated via selective laser sintering," *Biomaterials*, **26**, 4817–4827 (2005).
51. R. D. Goodridge, D. J. Wood, C. Ohtsuki, and K. W. Dalgarno, "Biological evaluation of an apatite–mullite glass-ceramic produced via selective laser sintering," *Acta Biomaterialia*, **3**, 221–231 (2007).
52. A. A. Krel' and L. N. Furtseva, "Methods for determining oxyproline in biological media and their use in clinical practices," *Vopr. Med. Khim.*, **6**, 635–640 (1968).